Onset of Darcy--Bénard convection under throughflow of a shear-thinning fluid

Onset of Darcy–Bénard convection under throughflow of a shear–thinning fluid

D. Petrolo[1], L. Chiapponi[1], S. Longo[1], M. Celli[2], A. Barletta[2], V. Di Federico[3]†

[1]Department of Engineering and Architecture - Università degli Studi di Parma - Parco Area delle Scienze 181/A - 43124 Parma - Italy

[2]Department of Industrial Engineering - Alma Mater Studiorum Università di Bologna - Viale Risorgimento 2 - 40136 Bologna - Italy

[3]Department of Civil, Chemical, Environmental, and Materials Engineering - Alma Mater Studiorum Università di Bologna - Viale Risorgimento 2 - 40136 Bologna - Italy

(Received xx; revised xx; accepted xx)

We present an investigation on the onset of Darcy–Bénard instability in a two–dimensional porous medium saturated with a non–Newtonian fluid and heated from below in presence of a uniform horizontal pressure gradient. The fluid is taken to be of power–law nature with constant rheological index n and temperature dependent consistency index μ^*. A two–dimensional linear stability analysis in the vertical plane yields the critical wave number and the generalised critical Rayleigh number as functions of dimensionless problem parameters, with a non monotonic dependence from n and with maxima/minima at given values of γ, a parameter representing the effects of consistency index variations due to temperature.

A series of experiments are conducted in a Hele-Shaw cell of aspect ratio $H/b = 13.3 - 20$ to provide a verification of the theory. Xanthan Gum mixtures (nominal concentration from 0.10% to 0.20%) are employed as working fluids with a parameter range $n = 0.55 - 0.72$ and $\mu_0^* = 0.02 - 0.10\,\mathrm{Pa\,s}^n$. The experimental critical wave number corresponding to incipient instability of the convective cells is derived via image analysis for different values of the imposed horizontal velocity. Theoretical results for critical wave number favourably compare with experiments, systematically underestimating their experimental counterparts by 10% at most. The discrepancy between experiments and theory is more relevant for the critical Rayleigh number, with theory overestimating the experiments by a maximum factor less than two. Discrepancies are attributable to a combination of factors: nonlinear phenomena, possible subcritical bifurcations, and unaccounted-for disturbing effects such as approximations in the rheological model, wall slip, ageing and degradation of the fluid properties.

1. Introduction

Thermal instability of saturated porous media has been intensively investigated with analytical tools (for a survey see Rees 2000; Nield & Bejan 2013) since the early studies of Horton & Rogers (1945) and Lapwood (1948), subsequently extended to include parallel horizontal flow (Prats 1966). Different combinations of boundary conditions are adopted in the literature for heat flux, temperature, and permeability (Nield 1968); the fluid is usually taken to be Newtonian.

Recent literature further broadens the analysis to cover non–Newtonian fluids, from power–law (Hirata & Ouarzazi 2010; Barletta & Nield 2011; Nield 2011*a*,*b*; Alloui *et al.*

† Email address for correspondence: vittorio.difederico@unibo.it

2012; Alves & Barletta 2013; Barletta & Storesletten 2016; Celli *et al.* 2017), to Bingham (Rees 2015) or viscoelastic (Hirata *et al.* 2015); this entails additional complexity deriving from fluid rheology.

From an experimental viewpoint, Rayleigh-Bénard convection in porous media has been studied by means of the Hele-Shaw analog model (see, e.g., Hartline & Lister 1977; Cherkaoui & Wilcock 2001; Letelier *et al.* 2016), originally developed for Newtonian fluids and recently extended to non–Newtonian power–law fluids (Longo *et al.* 2015; Ciriello *et al.* 2016): the porous medium is replaced with a small gap between two flat plates, this entails advantages and disadvantages. On one hand, experiments are easily prepared and the flow characteristics conveniently measured; on the other hand, simplifying assumptions on the structure of the simulated porous medium are needed. Direct experiments were performed simulating the porous medium with glass ballotini (see, e.g., Lister 1990; Keene & Goldstein 2015). The onset of convection in viscoplastic fluids, including the effects of wall slip, was analysed by Métivier & Magnin (2011) and Darbouli *et al.* (2013); a more complex scenario, with Carbopol behaving like a single or a double–phase continuum, has been analyzed in Métivier *et al.* (2017).

Several measurements techniques have been used for detecting the onset of instability, such as shadography (e.g., Darbouli *et al.* 2013), variation of thermal flux induced by convection (e.g., Schmidt & Milverton 1935), visualisation through a pH-indicator (Hartline & Lister 1977), magnetic resonance imaging (Shattuck *et al.* 1995), Digital Particle Image Velocimetry (DPIV) (Kebiche *et al.* 2014), holographic real–time interferometry (Koster & Müller 1982). Despite the accurate set up and the sophisticated instruments used, the overall accuracy in detecting instabilities is usually quite limited. This is partly a consequence of the fact that the dimensionless groups, relevant to describe the physical process of incipient convection, involve numerous variables, and each of these has its own uncertainty. In addition, detecting an instability at its onset is, by definition, a challenge: instabilities are linear at the very beginning, and induce a tiny modulation of velocity, thermal flux or refraction index. Detection of instabilities, however, takes place in many cases during the non–linear stage, whereas many theories refer to incipient linear instability.

For non–Newtonian fluids, additional complexities arise from measurement issues and uncertainty on rheological parameters, often in the presence of disturbing effects such as slipping, ageing and deterioration of the fluid under a prolonged thermal gradient. Further, most of the models adopted to describe non–Newtonian fluids are a strong simplification of the constituent equations, invariably referred to viscometric flow fields and subject to distortion in non–viscometric, complex 3-D flow fields. In this respect, there were some attempts to measure the rheological material properties in non conventional rheometers, like the experimental apparatus to be used for the main experiments in this work (Celli *et al.* 2017).

The aim of this work is comparing theoretical simulation with experimental results in Rayleigh–Bénard convection of a non–Newtonian power–law fluid within a vertical porous layer heated from below and subject to horizontal cross flow, a configuration common in several natural settings. The experimental set up is composed by a Hele–Shaw cell, and correspondingly the basic solution and linear stability analysis are derived for a two–dimensional geometry. The manuscript is structured as follows. Section 2 includes the mathematical formulation of the problem and the linear stability analysis. The experimental set up and the measurement techniques are described in Section 3, while Section 4 illustrates the experimental results. The discussion and the conclusions are presented in Section 5, together with some perspectives for future work. Supplementary material contains details on uncertainties of the experimental results.

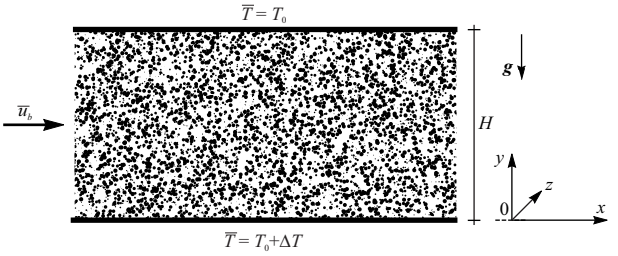

FIGURE 1. Sketch of the simulated domain.

2. Mathematical model

2.1. *Governing equations*

The theoretical simulation is focused on the two dimensional linear stability analysis of a fluid saturated horizontal porous layer of height H, see figure 1. The horizontal boundary planes are assumed to be impermeable and isothermal at temperature $T_0 + \Delta T$, lower boundary, and T_0, upper boundary. The Darcy's law generalised for non–Newtonian power–law fluids is here employed together with the Oberbeck-Boussinesq approximation. The local thermal equilibrium between the solid and the fluid phase is assumed and a convection–diffusion energy balance is used to model the heat transfer. The balance equations and the boundary conditions can be written in the dimensionless form,

$$\begin{gathered} \boldsymbol{\nabla} \cdot \mathbf{u} = 0, \\ \boldsymbol{\nabla} \times \left[\eta(T)\,|\mathbf{u}|^{n-1}\mathbf{u}\right] = Ra\,\boldsymbol{\nabla} \times (T\,\mathbf{e}_y)\,, \\ \frac{\partial T}{\partial t} + \mathbf{u} \cdot \boldsymbol{\nabla} T = \nabla^2 T, \\ y = 0: \quad v = 0,\ T = 1, \text{ and } \quad y = 1: \quad v = 0,\ T = 0, \end{gathered} \tag{2.1}$$

by introducing the transformations

$$(x, y) \to H\,(x, y), \quad (u, v) \to \frac{\varkappa}{H}(u, v), \quad t \to \frac{\sigma H^2}{\varkappa} t, \quad T \to (T_0 + \Delta T)T. \tag{2.2}$$

The Rayleigh number Ra is defined as

$$Ra = \frac{\rho_0\, g\, \beta\, \Delta T\, K\, H^n}{\mu_0^*\, \varkappa^n}. \tag{2.3}$$

Here, $\mathbf{u}$ is the seepage velocity having Cartesian components (u, v), (x, y) are the Cartesian coordinates with y denoting the vertical axis, T is the temperature, μ^* is the consistency index of the fluid and μ_0^* (SI unit [$\mathrm{Pa\,s^n}$]) denotes the value of μ^* evaluated at reference temperature T_0, n is the power–law index, K is the permeability with SI unit [$\mathrm{m^{n+1}}$], ρ_0 is the fluid density at the reference temperature T_0, $\mathbf{g}$ is the gravitational acceleration of modulus g, β is the thermal expansion coefficient of the fluid, σ is the ratio between the average volumetric heat capacity of the porous medium and the volumetric heat capacity of the fluid, $\varkappa$ is the average thermal diffusivity of the saturated porous medium. We assume here the following dependence of η on T (Nowak *et al.* 1982; Celli *et al.* 2017):

$$\eta(T) = \frac{\mu^*(T)}{\mu_0^*} = (1 + \gamma\, Ra\, T)^{-n}, \tag{2.4}$$

where γ is a non–negative dimensionless parameter that tunes the departure from the constant consistency index model, namely

$$\gamma = \frac{\mu_0^* \varkappa^n \xi}{\rho_0 g \beta K H^n}, \tag{2.5}$$

where ξ is a fluid property with unit $[\mathrm{K}^{-1}]$ modulating the slope of the temperature change. In passing, we note that an exponential dependence is modelled in Darbouli *et al.* (2016). A comparison between the two models is reported in the Supplementary material, showing that both models can be used, with a similar agreement between experimental data and interpolating function.

2.2. *Basic solution and stability analysis*

The stability analysis has to be performed on a stationary solution of the balance equations (2.1). This solution is the so–called basic state, here denoted by the subscript b. The stationary solution of eqs. (2.1) here considered as basic state is

$$u_b = Pe\left[1 + \frac{\gamma Ra\,(1-2y)}{2+\gamma Ra}\right], \quad v_b = 0, \qquad T_b = 1 - y, \tag{2.6}$$

where $\mathbf{u}_b = \{u_b, v_b\}$ is the basic state velocity vector, and the Péclet number is defined as the mean velocity of the basic flow given by

$$Pe = \int_0^1 u_b \,\mathrm{d}y. \tag{2.7}$$

As the experimental set up is composed by a Hele–Shaw cell, the basic state in eqs. (2.6) and (2.7) is two–dimensional. Accordingly, in the following, a two–dimensional linear stability analysis in the plane (x, y) is performed.
The basic state is thus perturbed by small–amplitude disturbances, namely

$$\mathbf{u} = \mathbf{u}_b + \varepsilon\,\mathbf{U}, \quad T = T_b + \varepsilon\,\Theta, \tag{2.8}$$

where $\mathbf{U} = (U, V)$ is the perturbation velocity, Θ is the perturbation temperature, and ε is a parameter such that $|\varepsilon| \ll 1$. The streamfunction, $\Psi(x, y)$, formulation can be employed to simplify the problem, with $U = \partial\Psi/\partial y$ and $V = -\partial\Psi/\partial x$. The perturbations can now be expressed in terms of normal modes, namely

$$\left\{ \begin{array}{c} \Psi(x,y,t) \\ \Theta(x,y,t) \end{array} \right\} = \left\{ \begin{array}{c} f(y) \\ h(y) \end{array} \right\} \exp(\lambda\, t) \exp\left[i\,(k\,x - \omega\, t)\right]. \tag{2.9}$$

One can substitute eqs. (2.8) and (2.9) into eqs. (2.1) to obtain

$$\begin{gathered} n(n-1)Gu_b' f' + nu_b\left[Gf'' + G'\left(f' - hu_b'\right)\right] - k^2 G u_b f - \\ u_b^2\left(G''h + G'h'\right) + ikRau_b^{2-n}h = 0, \\ h'' - h\left(k^2 + \lambda - i\omega + iku_b\right) - ikf = 0, \quad \text{with } f = 0, h = 0 \text{ at } y = 0, 1, \end{gathered} \tag{2.10}$$

where the primes denote derivatives with respect to y and $G(y) = \eta(T_b(y))$. We note that, due to eq. (2.10), we have $\mathrm{d}\eta(T_b)/\mathrm{d}T_b = -G'(y)$.

2.3. *Derivation of critical wave number and Rayleigh number*

The solution of eq. (2.10) is obtained numerically by employing the same procedure used in Celli *et al.* (2017). The critical values of the Rayleigh number and of the wave number are reported in figure 2 and figure 3 as functions of the parameter γ for different

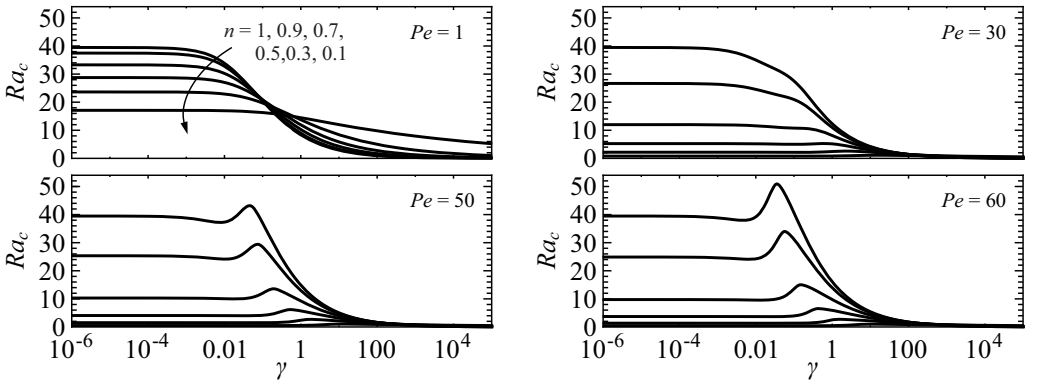

FIGURE 2. Critical values of the Rayleigh number.

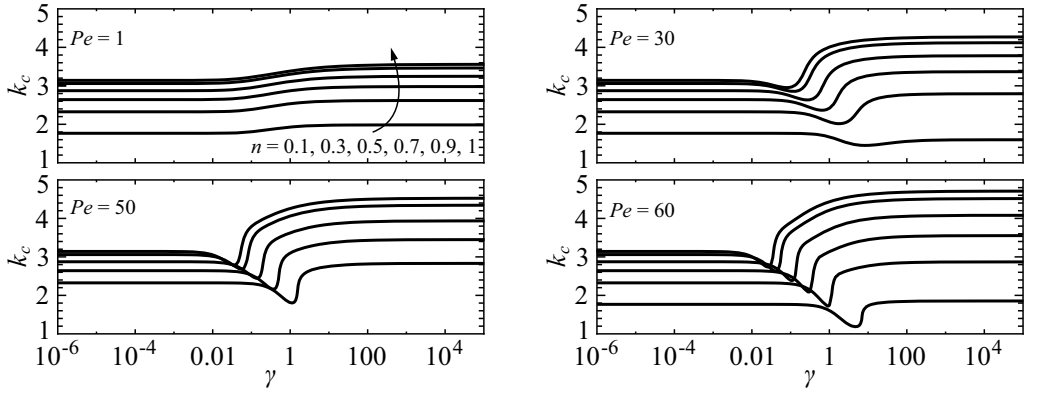

FIGURE 3. Critical values of the wave number.

values of the power–law index n and of the Péclet number. As Pe increases, these figures illustrate the non–monotonic behaviour of $Ra_{\rm cr}$ and $k_{\rm cr}$ versus γ.

3. Experimental set up

Validation of the model was performed by comparison of the theoretical results achieved in § 2 with experimental results obtained with an analogue model consisting of a Hele–Shaw cell 80 cm long and 4 cm high; its design is similar to Hartline & Lister (1977), see figures 4a-b. A frame of aluminium held together two polycarbonate windows 0.8 cm thick, with a gap variable between 0.1 and 0.3 cm controlled by aluminium shims. The upper and lower frames were cooled and heated, respectively, by a water flux within PVC pipes inserted into the frame. Temperature control within 0.1 K was achieved via two thermostatic baths. The temperature was measured with two probes inserted in the upper and lower side of the frame, PT100 4 wires AA 1/3DIN with a nominal accuracy of 0.1 K at 273 K. The probes where calibrated in a limited range of temperature with a maximum uncertainty of 0.08 K, hence the error on the temperature difference between the two frames is 0.12 K. The cell is insulated with foam rubbers in order to avoid lateral dispersion, except for a window in the central section to allow the observation of the fluid flow. The uniform horizontal velocity component, representing the basic flow, was obtained by injecting fluid with a syringe pump in one of the two wells, with overflow in the other well. The visualisation of the flow field was obtained with a tracer

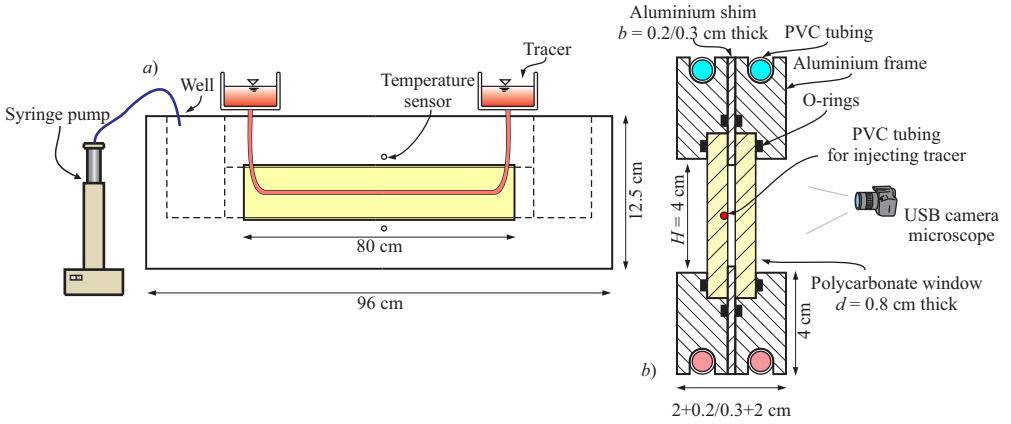

FIGURE 4. Layout of the Hele–Shaw cell.

having the same composition of the fluid within the cell, i.e. water and Xanthan Gum (nominal concentration in the range 0.10–0.20%, the real one is a little smaller because the mixture was filtered to eliminate some lumps for homogeneity), added with anyline dye. The tracer was injected through several small holes with diameter less than 0.1 mm in a PVC pipe inserted in one of the polycarbonate windows, positioned at mid-height of the window. The pipe was connected to two small tanks periodically refilled with tracer fluid, in order to guarantee a constant and uniform injection. The images were acquired with a USB video camera 1280×960 pixels with microscope lenses, with a field of view (FOV) of $\approx 12 \times 10$ cm^2. The FOV was enlightened with a lamp with rays made parallel through a lens, in order to increase resolution and sharpness. The video camera acquired a single frame each 30-60 s. The overall process was controlled by a PC with a DAQ board, storing temperature measurements at a data rate of 10 Hz, and controlling the USB image acquisition. Tracer was progressively injected and temperature set-up was increased/lowered for the hot/cold thermostatic bath, with steps of 0.1 K each 2-3 minutes. The variations of the upper/lower temperature were fixed in order to have a constant (or almost constant) temperature $T_{0.5}$ in the mid section. Most experiments lasted for 3-4 hours, with a time gradient of temperature of less than 10^{-3} K s^{-1}. A typical time series of measured temperatures is shown in the Supplementary material, as well as details on rheometric measurements and experimental uncertainties.

4. Experimental results

The experiments and their parameters are listed in Table 1. Figure 5 shows a typical sequence of frames from the early stages of instabilities development to the appearance of strongly non–linear instabilities. A slow translation to the left is observed due to the basic flow velocity of 0.0087 cm s^{-1}. Similar results were obtained for all tests. In most cases, the temperature difference between the two frames first showed an increase over time, followed by a reduction, with consequent linearisation of the convective cells up to their disappearance. Hysteresis phenomena, with a difference in temperature at the early appearance of the cell (branch of rising ΔT) higher than the difference in temperature corresponding to the return to stability (branch of reducing ΔT), were evident only for the more viscous fluid flow. The description of the methodology adopted for comparison gives evidence of the numerous experimental complexities encountered during the activity.

Figure 6*a*-*b* shows the comparison between theoretical and experimental critical

Expt.	ρ_0 ($\mathrm{g\,cm^{-3}}$)	μ_0^* ($\mathrm{Pa\,s^n}$)	n	b (cm)	$\overline{u}_b$ ($\mathrm{cm\,s^{-1}}$)	$T_{0.5}$ (K)	Pe	$Ra_{c,exp}$	$k_{c,exp}$
1	1.003	0.02	0.72	0.2	0.0131	298.2-298.4	52 ± 2	9.8 ± 0.4	2.96 ± 0.07
2	1.003	0.10	0.55	0.2	0.0131	298.3-299.1		6.2 ± 0.6	2.99 ± 0.07
3	1.003	0.05	0.60	0.2	0.0131	298.5-298.7		4.8 ± 0.4	2.80 ± 0.06
4	1.003	0.07	0.66	0.2	0.0131	298.3-299.0		8.3 ± 0.8	2.86 ± 0.06
5	1.003	0.05	0.60	0.3	0.0087	298.7-298.9	34 ± 2	4.0 ± 0.4	2.94 ± 0.07
6	1.003	0.07	0.66	0.3	0.0087	298.9-299.1		6.3 ± 0.4	3.05 ± 0.07
7	1.003	0.10	0.55	0.3	0.0087	298.7-299.2		4.7 ± 0.6	2.78 ± 0.06

TABLE 1. Parameters of the experiments. ρ_0 is the reference mass density at the temperature of 298 K, μ_0^* is the fluid consistency index evaluated at the reference temperature T_0, n is the fluid behaviour index, b is the gap width, $\overline{u}_b$ is the average basic horizontal velocity, $T_{0.5}$ is the temperature in the mid section $z/H = 0.5$ during experiments (minimum/maximum value), Pe is the Péclet number, $Ra_{c,exp}$ is the experimental critical Rayleigh number, $k_{c,exp}$ is the dimensionless critical wave number.

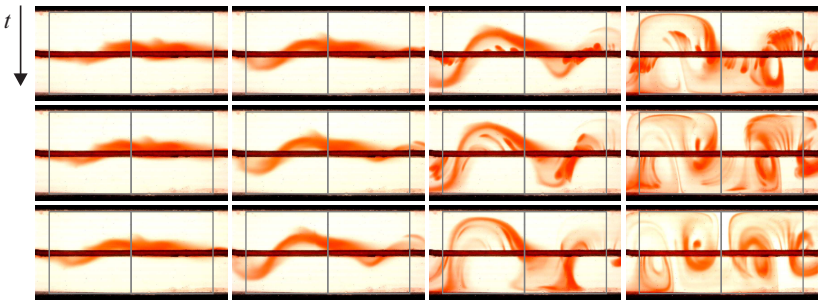

FIGURE 5. Evolution of the perturbation over time (top to bottom and left to right) for one of the experiments. The vertical lines delimit squares with side length equal to $H = 4\,\mathrm{cm}$. In the last frame (bottom–right) a bifurcation of the cell in a strongly non–linear regime is observed. Snapshots are 60 s apart.

Rayleigh number for two different groups of experiments with different values of the Péclet number Pe. The error bars are shown for the experiments and represent one standard deviation. The theoretical predictions are supplemented with confidence limits corresponding to the possible combinations of the variables and parameters involved in the model, assumed equal to their nominal value plus/minus their standard deviation.

The value of theoretical Ra_c increases for increasing fluid behaviour index, although not monotonically for the larger value of Pe considered; also, an increase in Pe brings about an increase in Ra_c, albeit not in the same proportion for different values of n. These theoretical values consistently over–predict experimental values to various degrees, from around 15% to nearly 100%; no clear trend is detected in the discrepancy for different values of n and/or Pe. The experimental values of Ra_c obtained show a non monotonic behaviour with fluid behaviour index n; for both Pe values, a minimum for Ra_c is evident at $n = 0.6$.

Figure 6*c-d* compares also the experimental and theoretical values of the critical wave number for varying n, again for two different values of Pe. The trend is correctly reproduced and the theoretical formulation always under-predicts the experimental result to a variable degree (the maximum discrepancy is below 10%), with a lower average discrepancy for experiments at low Péclet number.

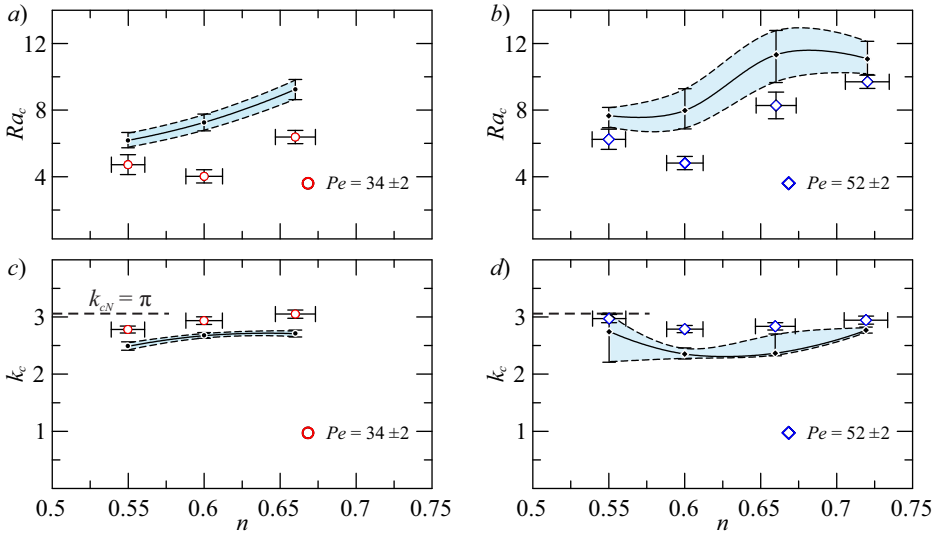

FIGURE 6. Comparison of the experimental and theoretical values of the critical Rayleigh number *a*) for $Pe = 34 \pm 2$ and *b*) for $Pe = 52 \pm 2$, and of the critical wave number *c*) for $Pe = 34 \pm 2$ and *d*) for $Pe = 52 \pm 2$. Open symbols are the experiments, curves are theory. The error bars and the confidence bands refer to one standard deviation. $k_{cN} = \pi$ is the critical wave number for a Newtonian fluid initially at rest.

There are several sources of discrepancy: the strong non–linearity of the flow field favours a rapid evolution of the cell from the onset of instability towards a fully developed cell with a reduction of wavelength (and consequent increment of the experimental wave number). A further evolution brings to doubling of the cells. A disturbing factor is a possible slip at the wall, which is not included in the model and which reduces the flow resistance and favours the growth of the instability. This effect was clearly detected for viscoplastic fluids (Darbouli *et al.* 2013) and is widely documented for most aqueous polymer solutions, see Joshi *et al.* (2000); Valdez *et al.* (1995).

5. Discussion and conclusions

The need to extend the available models for Darcy–Bénard instability to rheologically complex fluids and non–viscometric flow fields has suggested the analysis of non–Newtonian fluid flow in a two–dimensional geometry and in the presence of a uniform cross flow. The fluid is assumed to display a power–law nature with temperature dependent consistency index. A two–dimensional linear stability analysis in the vertical plane yields the critical wave number and the critical Rayleigh number upon solving numerically the eigenvalue problem. The critical Rayleigh and wave numbers are significantly affected by the power–law index and by the thermal effects on the consistency index, displaying a non–monotonic trend with local minima and maxima.

A set of experiments performed in a Hele–Shaw cell allowed to study flow patterns as functions of the Rayleigh number. The experiments were carried out with shear thinning fluids of flow behaviour index n ranging from 0.55 to 0.72, coupled with cell gap–widths of 0.2 or 0.3 cm, imposing cross flow velocities around 0.01 $\mathrm{cm\,s^{-1}}$ and vertical temperature gradients of $0.5 - 3.4$ $\mathrm{K\,cm^{-1}}$ between the lower and upper frames. The critical wave number was obtained via analysis of the frames acquired.

The overall flow dynamics is controlled by the entangled interaction between fluid properties, geometry of the flow field and underlying uniform cross flow. The onset of convective cells occurs with increasing wave number for increasing n. At the onset of convection, the shear–thinning behaviour favours a fast growth of the instabilities. Considering the complexity of the protocol and the numerous sources of uncertainty (see Longo *et al.* 2013*b*, for details on uncertainties in rheometric measurements), experimental results show a fairly good agreement, within 10%, with theory for the critical wave number. The discrepancy may be attributed to nonlinear phenomena not captured by the linear stability analysis, and additionally to slip at the wall, and ageing and degradation of the fluid properties, all unaccounted-for phenomena in the theoretical model.

Results for the critical Rayleigh number show a correct trend and an overall acceptable agreement with theoretical predictions; the discrepancy varies widely with n and Pe values and is generally larger than for the critical wave number. The theoretical model itself shows a larger sensitivity to the governing parameters for Ra_c than for k_c. Other rheological models, more complex than the power-law, are available to describe Xanthan Gum mixtures (see, e.g. Escudier *et al.* 2001, where a Carreau-Yasuda model is favourably tested). However, the power-law model is suitable to locally describe complex rheologies, with several validations in complex flows geometries, see Longo *et al.* (2013*a*) and the recent Chiapponi *et al.* (2019). In this regard, we have verified that in the shear rate range of our experiments, a power-law model adequately fits the rheometric data, see Figure 1b and its caption in the Supplementary material.

The experiments showed clearly that the development of the instability may occur at a threshold Rayleigh number lower than the critical value predicted by linear stability theory. This could be considered as symptomatic of a subcritical bifurcation, induced by the nonlinear terms in the governing equations of the fluid. Indeed, it is well established, both experimentally and theoretically, that the bifurcation is supercritical in the Darcy-Bénard convection with throughflow for a Newtonian fluid. The supercritical linear threshold of absolute instability (see Barletta 2019) was found to correspond perfectly to the one needed in experiments to trigger the instability. As suggested by the present series of experiments, as well as by the shear-thinning behaviour (see Balmforth & Rust 2009; Albaalbaki & Khayat 2011; Bouteraa *et al.* 2015), the nature of the bifurcation may be subcritical, and therefore a nonlinear stability analysis has to be carried out as a natural development of the present study. By using the concepts of nonlinearly convective and absolute instability, as defined in Couairon & Chomaz (1997), one can hope to obtain results that corroborate the experimental results obtained in this paper.

The present study can be extended in several directions. In particular, a change of the boundary condition (open instead of closed top) in the experimental setup could give further hints for understanding the complex evolution of the cells; a direct numerical simulation should be at hands, due to the viscous regime of the flow field. The great flexibility of numerical experiments could shed light on the possible effects of slip at the wall and on the evolution in quasi–linear and fully non–linear regime. Additional topics to be investigated are related to vertical fractures with uneven gap (e.g., see Felisa *et al.* 2018), which are good proxies of geological fractures characterised by a length scale from a few centimetres to several metres and subject to thermal gradients and cross flow. The vertical convection should be a quite efficient agent for re–mixing the fluid, favouring heat exchange and chemical reactions.

Acknowledgements

Sandro Longo gratefully acknowledges the financial support from Anton Paar for co-funding Anton Paar MCR702 rheometer. The cost of the equipment used for this experimental investigation was partly supported by the University of Parma through the Scientific Instrumentation Upgrade Programme 2018. Vittorio Di Federico gratefully acknowledges financial support from Università di Bologna Almaidea 2017 Linea Senior grant.

REFERENCES

Albaalbaki, Bashar & Khayat, Roger E 2011 Pattern selection in the thermal convection of non-newtonian fluids. *Journal of Fluid Mechanics* **668**, 500–550.

Alloui, Z., Khelifa, N. B., Beji, H. & Vasseur, P. 2012 Onset of convection in a horizontal porous layer saturated by a power-law fluid. *Journal of Heat Transfer* **134** (9), 092502.

Alves, L. S. de B. & Barletta, A. 2013 Convective instability of the Darcy-Bénard problem with through flow in a porous layer saturated by a power-law fluid. *International Journal of Heat and Mass Transfer* **62**, 495–506.

Balmforth, N. J. & Rust, A. C. 2009 Weakly nonlinear viscoplastic convection. *Journal of Non-Newtonian Fluid Mechanics* **158** (1-3), 36–45.

Barletta, A. 2019 *Routes to Absolute Instability in Porous Media*. Springer.

Barletta, A. & Nield, D. A. 2011 Linear instability of the horizontal throughflow in a plane porous layer saturated by a power-law fluid. *Physics of Fluids* **23**, 013102.

Barletta, A. & Storesletten, L. 2016 Linear instability of the vertical throughflow in a horizontal porous layer saturated by a power-law fluid. *International Journal of Heat and Mass Transfer* **99**, 293–302.

Bouteraa, M., Nouar, C., Plaut, E., Métivier, C. & Kalck, A. 2015 Weakly nonlinear analysis of rayleigh–bénard convection in shear-thinning fluids: nature of the bifurcation and pattern selection. *Journal of Fluid Mechanics* **767**, 696–734.

Celli, M., Barletta, A., Longo, S., Chiapponi, L., Ciriello, V., Di Federico, V. & Valiani, A. 2017 Thermal instability of a power-law fluid flowing in a horizontal porous layer with an open boundary: a two-dimensional analysis. *Transport in Porous Media* **118** (3), 449–471.

Cherkaoui, A. S. M. & Wilcock, W. S. D. 2001 Laboratory studies of high Rayleigh number circulation in an open-top Hele-Shaw cell: An analog to mid-ocean ridge hydrothermal systems. *Journal of Geophysical Research: Solid Earth* **106**, 10983–11000.

Chiapponi, L., Ciriello, V., Longo, S. & Di Federico, V. 2019 Non-Newtonian backflow in an elastic fracture. *Water Resources Research* **n/a** (n/a), , arXiv: https://agupubs.onlinelibrary.wiley.com/doi/pdf/10.1029/2019WR026071.

Ciriello, V., Longo, S., Chiapponi, L. & Di Federico, V. 2016 Porous gravity currents: a survey to determine the joint influence of fluid rheology and variations of medium properties. *Advances in Water Resources* **92**, 105–115.

Couairon, A. & Chomaz, J.-M. 1997 Absolute and convective instabilities, front velocities and global modes in nonlinear systems. *Physica D: Nonlinear Phenomena* **108** (3), 236–276.

Darbouli, M., Métivier, C., Leclerc, S., Nouar, C., Bouteera, M. & Stemmelen, D. 2016 Natural convection in shear-thinning fluids: Experimental investigations by MRI. *International Journal of Heat and Mass Transfer* **95**, 742–754.

Darbouli, M., Métivier, C., Piau, J.-M., Magnin, A. & Abdelali, A. 2013 Rayleigh-Bénard convection for viscoplastic fluids. *Physics of Fluids* **25**, 023101.

Escudier, M. P., Gouldson, I. W., Pereira, A. S., Pinho, F. T. & Poole, R. J. 2001 On the reproducibility of the rheology of shear-thinning liquids. *Journal of Non-Newtonian Fluid Mechanics* **97** (2-3), 99–124.

Felisa, G., Lenci, A., Lauriola, I., Longo, S. & Di Federico, V. 2018 Flow of truncated power-law fluid in fracture channels of variable aperture. *Advances in Water Resources* **122**, 317–327.

Hartline, B. K. & Lister, C. R. B. 1977 Thermal convection in a Hele-Shaw cell. *Journal of Fluid Mechanics* **79**, 379–389.

Hirata, S. C., Alves, L. S. de B., Delenda, N. & Ouarzazi, M. N. 2015 Convective and absolute instabilities in Rayleigh–Bénard–Poiseuille mixed convection for viscoelastic fluids. *Journal of Fluid Mechanics* **765**, 167–210.

Hirata, S. C. & Ouarzazi, M. N. 2010 Three-dimensional absolute and convective instabilities in mixed convection of a viscoelastic fluid through a porous medium. *Physics Letters A* **374**, 2661–2666.

Horton, C. W. & Rogers, F. T. 1945 Convection currents in a porous medium. *Journal of Applied Physics* **16**, 367–370.

Joshi, Y. M., Lele, A. K. & Mashelkar, R. A. 2000 Slipping fluids: a unified transient network model. *Journal of non-Newtonian Fluid Mechanics* **89** (3), 303–335.

Kebiche, Z., Castelain, C. & Burghelea, T. 2014 Experimental investigation of the Rayleigh–Bénard convection in a yield stress fluid. *Journal of Non-Newtonian Fluid Mechanics* **203**, 9–23.

Keene, D. J. & Goldstein, R. J. 2015 Thermal Convection in Porous Media at High Rayleigh Numbers. *Journal of Heat Transfer* **137**, 034503.

Koster, J. N. & Müller, U. 1982 Free convection in vertical gaps. *Journal of Fluid Mechanics* **125**, 429–451.

Lapwood, E. R. 1948 Convection of a fluid in a porous medium. *Proceedings of the Cambridge Philosophical Society* **44**, 508–521.

Letelier, J. A., Herrera, P., Mujica, N. & Ortega, J. H. 2016 Enhancement of synthetic schlieren image resolution using total variation optical flow: application to thermal experiments in a Hele-Shaw cell. *Experiments in Fluids* **57**, 1–14.

Lister, C. R. B. 1990 An explanation for the multivalued heat transport found experimentally for convection in a porous medium. *Journal of Fluid Mechanics* **214**, 287–320.

Longo, S., Di Federico, V., Archetti, R., Chiapponi, L., Ciriello, V. & Ungarish, M. 2013*a* On the axisymmetric spreading of non-Newtonian power-law gravity currents of time-dependent volume: an experimental and theoretical investigation focused on the inference of rheological parameters. *Journal of Non-Newtonian Fluid Mechanics* **201**, 69–79.

Longo, S., Di Federico, V. & Chiapponi, L. 2015 A dipole solution for power-law gravity currents in porous formations. *Journal of Fluid Mechanics* **778**, 534–551.

Longo, S., Di Federico, V., Chiapponi, L. & Archetti, R. 2013*b* Experimental verification of power-law non-Newtonian axisymmetric porous gravity currents. *Journal of Fluid Mechanics* **731**, R2.

Métivier, C., Li, C. & Magnin, A. 2017 Origin of the onset of Rayleigh-Bénard convection in a concentrated suspension of microgels with a yield stress behavior. *Physics of Fluids* **29** (10), 104102.

Métivier, C. & Magnin, A. 2011 The effect of wall slip on the stability of the Rayleigh–Bénard Poiseuille flow of viscoplastic fluids. *Journal of Non-Newtonian Fluid Mechanics* **166** (14), 839 – 846.

Nield, D. A. 1968 Onset of thermohaline convection in a porous medium. *Water Resources Research* **11**, 553–560.

Nield, D. A. 2011*a* A further note on the onset of convection in a layer of a porous medium saturated by a non-Newtonian fluid of power-law type. *Transport in Porous Media* **88**, 187–191.

Nield, D. A. 2011*b* A note on the onset of convection in a layer of a porous medium saturated by a non-Newtonian nanofluid of power-law type. *Transport in Porous Media* **87**, 121–123.

Nield, D. A. & Bejan, A. 2013 *Convection in Porous Media*, 4th edn. New York: Springer-Verlag.

Nowak, Z., Gryglaszewski, P. & Stacharska-Targosz, J. 1982 Laminar heat transfer to power law fluids in flat gaps with various thermal wall conditions. *Acta Mechanica* **44**, 223–236.

Prats, M. 1966 The effect of horizontal fluid flow on thermally induced convection currents in porous mediums. *Journal of Geophysical Research* **71**, 4835–4838.

Rees, D. A. S. 2000 The stability of Darcy–Bénard convection. In *Handbook of Porous Media* (ed. K. Vafai & H. A. Hadim), chap. 12, pp. 521–558. New York: CRC Press.

Rees, D. A. S. 2015 Convection of a Bingham fluid in a porous medium. In *Handbook of Porous Media*, 3rd edn. (ed. K. Vafai), chap. 17, pp. 559–595. CRC Press.

Schmidt, R. J. & Milverton, S. W. 1935 On the instability of a fluid when heated from below. *Proceedings of the Royal Society of London. Series A-Mathematical and Physical Sciences* **152** (877), 586–594.

Shattuck, M. D., Behringer, R. P., Johnson, G. A. & Georgiadis, J. G. 1995 Onset and stability of convection in porous media: Visualization by magnetic resonance imaging. *Physical Review Letters* **75** (10), 1934.

Valdez, M. A., Yeomans, L., Montes, F., Acuña, H. & Ayala, A. 1995 Influence of temperature on the slip velocity of semidilute Xanthan Gum solutions. *Rheologica Acta* **34** (5), 474–482.